Optics Communications 329 (2014) 76–80

Contents lists available at ScienceDirect

Optics Communications

journal homepage: www.elsevier.com/locate/optcom

A circuit method to integrate metamaterial and graphene in absorber design

Zuojia Wang [a,b,1], Min Zhou [c,1], Xiao Lin [a,b], Huixia Liu [a,b], Huaping Wang [c,*], Faxin Yu [c], Shisheng Lin [b], Erping Li [b], Hongsheng Chen [a,b,**]

[a] The Electromagnetics Academy at Zhejiang University, Zhejiang University, Hangzhou 310027, China
[b] Department of Information Science and Electronic Engineering, Zhejiang University, Hangzhou 310027, China
[c] School of Aeronautics and Astronautics, Zhejiang University, Hangzhou 310027, China

ARTICLE INFO

Article history:
Received 15 January 2014
Received in revised form
7 April 2014
Accepted 3 May 2014
Available online 14 May 2014

Keywords:
Metamaterial
Graphene
Integration
tunability
Absorber

ABSTRACT

We theoretically investigate a circuit analog approach to integrate graphene and metamaterial in electromagnetic wave absorber design. In multilayer graphene-metamaterial (GM) absorbers, ultrathin metamaterial elements are theoretically modeled as equivalent loads which attached to the junctions between two transmission lines. Combining with the benefits of tunable chemical potential in graphene, an optimized GM absorber is proposed as a proof of the circuit method. Numerical simulation results demonstrate the effectiveness of the circuit analytical model. The operating frequency of the GM absorber can be varied in terahertz frequency, indicating the potential applications of the GM absorber in sensors, modulators, and filters.

1. Introduction

A perfect electromagnetic (EM) wave absorber is a device to absorb all incident radiation at the operating frequency and to disable all other light propagation channels [1]. Salisbury screen based on the transmission line theory is the fundamental strategy to design EM absorbers in which a resistive sheet is placed in front of a metal ground plane with a distance of one fourth of the wavelength [2]. As a broadband extension of the Salisbury screen, the Jaumann absorber consists of two or more resistive sheets and resonances over multiple wavelengths [2]. To achieve high absorption over broad band, circuit analog (CA) absorbers are developed in which lossy frequency selective surfaces (FSS) are arranged periodically in front of a single metal ground [3,4]. With its rapid developments in artificial materials, metamaterials are recently proposed to design novel EM absorbers [5–10]. Unlike conventional absorbers based on transmission line theory, metamaterials, consisting of solely metallic elements, are usually described as effective materials via effective electric permittivity and effective magnetic permeability [11–15]. By independently tuning the resonance in ε and μ, metamaterials can be designed with matched impedance to free space, thus realizing approximately zero reflectivity [5]. This seminal work soon has inspired other works in various frequency regimes. High absorptivity has been achieved in THz [16], mid-infrared [17], near-infrared [18] and visible [19] frequencies.

Graphene [20–22], one-atom-thick electromagnetic material with the flexible tunability of its chemical potential [23], is a promising two-dimensional platform of designing atomically-thick plasmonics and metamaterials [24–26]. In particular, some works have already shown the good optical absorption performance of graphene sheets [27–30]. However, combining graphene with conventional metamaterials to establish novel EM absorbers has been rarely discussed [27–30]. In this paper, basing on transmission line theory, we propose a circuit analog method to integrate graphene and metamaterial sheets in absorber design, which may provide theoretical guidance for designing graphene-metamaterial (GM) combined absorbers. As a proof of concept, an optimized tunable GM absorber, whose operating frequency can be varied from 1.77 THz to 2.59 THz, is proposed.

2. Results and discussion

The GM absorber under consideration consists of a metamaterial sheet and a graphene sheet separated by insulators (polymer) located upon a metal ground plane. Two typical structures are

* Corresponding author.
** Corresponding author at: The Electromagnetics Academy at Zhejiang University, Zhejiang University, Hangzhou 310027, China.
E-mail addresses: hpwang78@gmail.com (H. Wang), hansomchen@zju.edu.cn (H. Chen).
[1] Co-first authors.

http://dx.doi.org/10.1016/j.optcom.2014.05.010
0030-4018/

schematically shown in Fig. 1. The unit cells of both the graphene-embedded (in Fig. 1(a)) and metamaterial-embedded (in Fig. 1(b)) structures are periodically arranged along the x and y directions with the periodicity, $p = 20\ \mu m$. The patterned metamaterial film (cut-wire shape) is constructed by copper whose thickness is $t_m = 0.02\ \mu m$. In the graphene-embedded sample, a graphene sheet is sandwiched between two polymer layers (with different thicknesses d_1,d_2) and the metamaterial film is placed on the top. Whereas, the metamaterial-embedded sample has a reverse arrangement in which the top layer is a graphene sheet. It should be noted that throughout this paper the time variation is $e^{j\omega t}$, where j is the imaginary unit.

Based on transmission line theory, an effective circuit analog model is established in Fig. 1(c), where ε_0 is the dielectric constant of vacuum, $\varepsilon_p = 3.5\varepsilon_0$ represents the dielectric constant of polymer. Due to the ultrathin thicknesses compared with the operating wavelength, both the graphene sheet and the metamaterial film can be treated as conductive films with the surface impedances Z_g and Z_m, respectively. Polymer layers, modeled as transmission lines, can be designed either inductive or capacitive to satisfy desired absorption performance. Without lose generality, consider wave is obliquely incident onto the GM absorber with an incident angle of θ, the effective circuit parameters shown in Fig. 1(c) for TE polarization (the electric field is along x axis) in metamaterial-embedded structures are derived as [31]

$$Z_1 = jZ_p \tan(k_{zp}d_1) \quad (1)$$

$$Z_2 = (Z_1 Z_m)/(Z_1 + Z_m) \quad (2)$$

$$Z_3 = Z_p(Z_2 + jZ_p \tan(k_{zp}d_2))/(Z_p + jZ_2 \tan(k_{zp}d_2)) \quad (3)$$

$$Z_{in} = (Z_3 Z_g)/(Z_3 + Z_g) \quad (4)$$

where $Z_p = \omega\mu_0/k_{zp}$ is the characteristic impedance of the polymer, $k_{zp} = \sqrt{k_p^2 - k_0^2 \sin^2\theta}$ is the propagation constant along z-direction, and $k_p = \omega\sqrt{\mu_0\varepsilon_p}$ is the wave number in the polymer.

To evaluate the absorbing performance of such proposed GM combined absorbers, the impedances of the graphene sheets ($Z_g = 1/\sigma_g$) and the metamaterial films ($Z_m = 1/\sigma_m^{eff}$) are compulsory to calculate, where σ_g and σ_m^{eff} are the effective surface conductivities of graphene and the metamaterial, respectively. Note that graphene

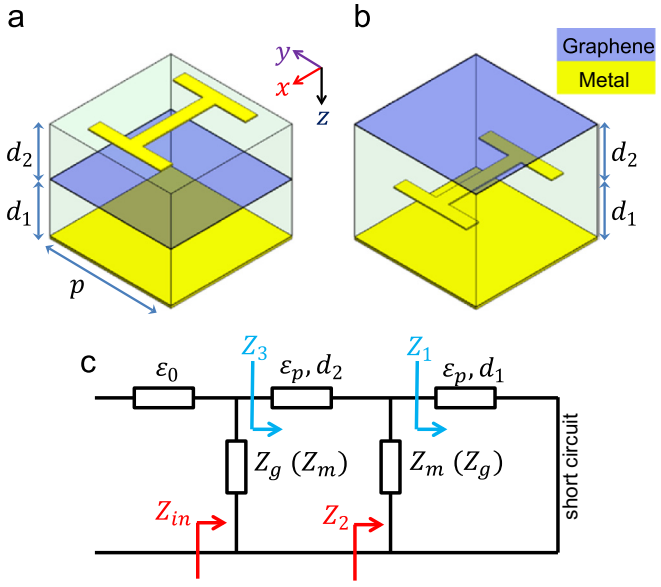

Fig. 1. The schematic diagram of the GM absorbers. (a) Graphene-embedded structure, (b) metamaterial-embedded structure, and (c) equivalent circuit model.

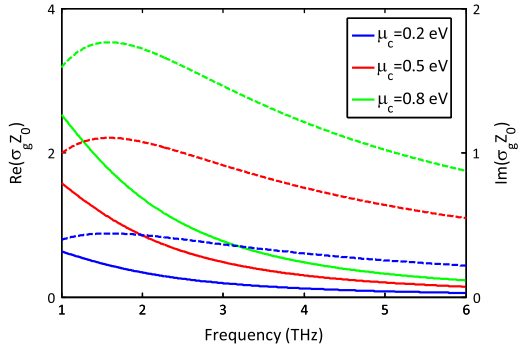

Fig. 2. Normalized surface optical conductivity of graphene with various chemical potentials. The solid and dashed lines correspond to the real and imaginary parts of $\sigma_g Z_0$, respectively.

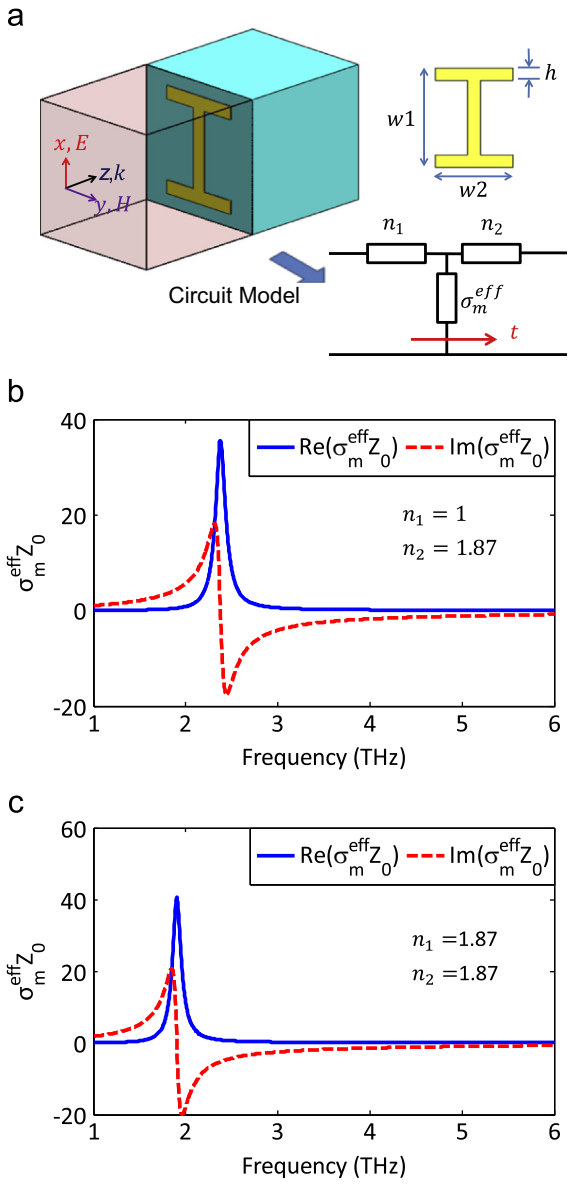

Fig. 3. (a) The equivalent circuit model of a metamaterial film sandwiched in dielectrics. The retrieved effective electric sheet conductivity for (b) $n_1 = 1$, $n_2 = 1.87$, and (c) $n_1 = n_2 = 1.87$.

is usually characterized by its surface conductivity [32–34], which can be calculated directly by the Kubo formula [35–38]

$$\sigma_g(\omega,\mu_c,\tau,T)=\frac{je^2(\omega-j\tau^{-1})}{\pi\hbar^2}\left[\int_{-\infty}^{+\infty}\frac{|\varepsilon|}{(\omega-j\tau^{-1})^2}\frac{\partial f_d(\varepsilon)}{\partial\varepsilon}d\varepsilon - \int_0^{+\infty}\frac{\partial f_d(-\varepsilon)-\partial f_d(\varepsilon)}{(\omega-j\tau^{-1})^2-4(\varepsilon/\hbar)^2}d\varepsilon,\right] \quad (5)$$

where $f_d=1/(1+\exp[(\varepsilon-\mu_c)/k_BT])$ is the Fermi–Dirac distribution, μ_c is the chemical potential, e is the electron charge, $\hbar$ is the reduced Planck's constant, k_B is the Boltzmann's constant, and τ is the momentum relaxation time due to the carrier intraband scattering. The first term in Eq. (5) corresponds to the intraband electron–photon scattering process and the second term relates to the direct interband electron transition. For simplicity, we use here a constant value of $\tau=0.1$ ps. At THz regime, when $\hbar\omega\ll|\mu_c|$, the interband part in Eq. (5) is negligible and the surface conductivity can be simplified as [37,39]

$$\sigma_g\approx\sigma_{intra}=\frac{-je^2k_BT}{\pi\hbar^2(\omega-j\tau^{-1})}\left[\frac{\mu_c}{k_BT}+2\ln\left(\exp\left(-\frac{\mu_c}{k_BT}\right)+1\right).\right] \quad (6)$$

At room temperature (T=300 K), Fig. 2 shows the normalized surface conductivity (σ_gZ_0) of monolayer graphene with various chemical potentials (0.2–0.8 eV), where $Z_0=120\pi$ ohm is the free-space impedance. In the frequency range of 1–6 THz, the higher μ_c has larger graphene's conductivity, which shows promising applications in realizing tunable absorbers and other switchable devices with a voltage-controllable effect.

Theoretically calculating the conductivity of patterned metmaterials is much more difficult, instead, we use a viable numerical method to retrieve its effective parameters. It has been proven that thin-film metamaterial and conductivity sheets can be characterized with the electric and magnetic effective surface conductivity [40]. Therefore, in this context, a similar retrieval approach is employed to calculate the effective electric surface conductivity of the metamaterial film sandwiched in different dielectrics. For simplicity, a non-magnetic resonance metamtarial film is adopted. The unit cell of the considered metamaterial (Fig. 3a) consists of a cut-wire made of copper whose dimensions are $w_1=19\ \mu m$, $w_2=10\ \mu m$, and $h=0.6\ \mu m$. This metamaterial film between two dielectrics is equivalent to a load attached to the junctions between two transmission lines. In the case of normal incidence, the effective surface electric conductivity of the metamaterial film (σ_m^{eff}) can be expressed as [41,42]

$$\sigma_m^{eff}=\frac{1}{Z_0}\left(\frac{2n_1}{t}-(n_1+n_2)\right), \quad (7)$$

where n_1 and n_2 are the refractive indices of the cladding and substrate, respectively, t is the transmission coefficient for a normal incident wave coming from the cladding (n_1). The scattering parameters are calculated by a frequency-domain electromagnetic solver. One unit cell is stimulated with mirror symmetry boundary conditions (PEC/PMC) to model a period array of cut-wires. The incident electric field is along the x direction. The retrieved effective electric sheet conductivities ($\sigma_m^{eff}=\mathrm{Re}(\sigma_m^{eff})+j\mathrm{Im}(\sigma_m^{eff})$) of the metamaterial films in different backgrounds following Eq. (7) are plotted in Fig. 3(b) and (c). One can see that the electric sheet conductivities have noticeable Lorentz resonances and hence the incident waves will be highly scattered at resonance frequencies [40]. The resonance frequency of the cut-wire metamaterial shifts from 2.38 THz to 1.9 THz when the refractive index of cladding substrates changes from 1 to 1.87. Therefore, the influence of substrates should be considered when using the circuit analog approach to design metamaterial devices.

Based on the aforementioned parameters of the graphene sheet and the metamaterial film, we are now going to verify the validity of our proposed circuit analog method in designing GM absorbers. Fig. 4 shows the simulated and theoretical results of the reflection coefficients for GM absorbers with $\mu_c=0.5$ eV. The geometry parameters we adopted here are consistent to previous description except for $d_1=d_2=10\ \mu m$. In the simulation, we simulated the whole structure in microwave CST. These curves show that the simulation results are highly consistent with the theoretical results. In the simulation, two absorbing peaks exist for both the metamaterial-embedded structure and the graphene-embedded structure. Meanwhile, the absorbing frequencies experience shifts

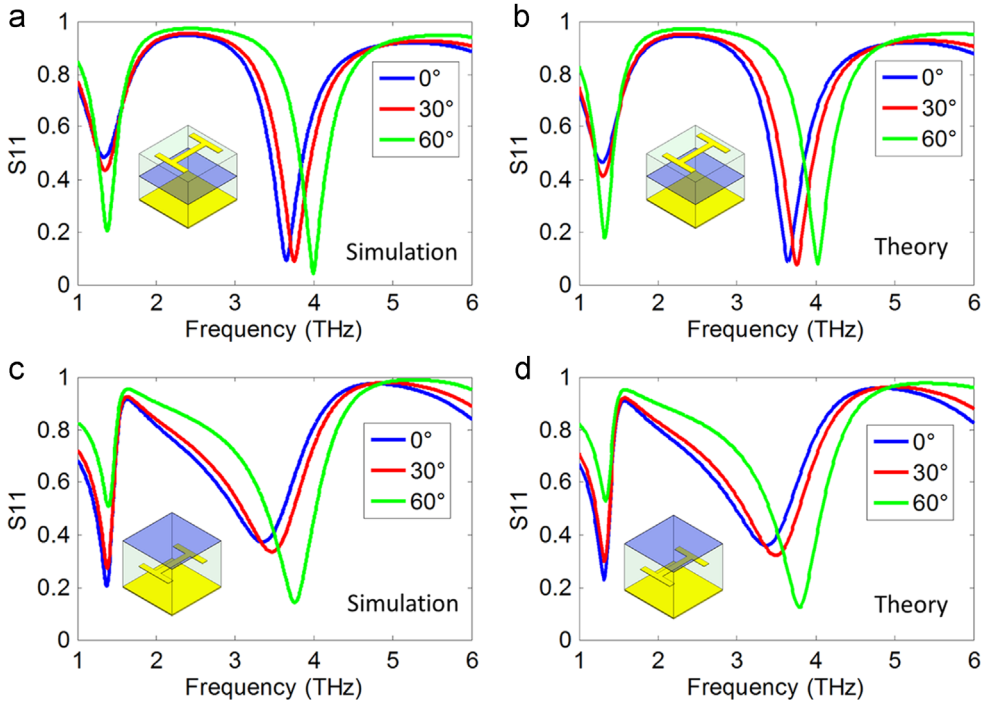

Fig. 4. Simulated and theoretical reflection coefficients for (a and b) the graphene-embedded structure and (c and d) the metamaterial-embedded structure.

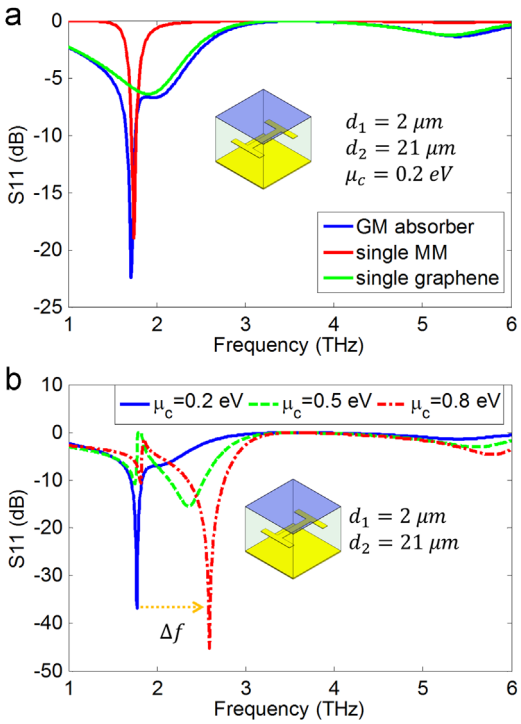

Fig. 5. (a) Reflection coefficients for the optimized GM aborber and the structures comprising single metamaterial or single graphene. (b) Similar plot varying the chemical potential.

for different incident angles. The underlying reason is that the input impedance, related to the propagation constant along z-direction, is sensitive to the incidence angle.

Rooted on these understandings, tunable devices with desired properties based on circuit analog approach can be designed. Specially, to demonstrate the potential of circuit analog method, we propose an optimized GM absorber, using the metamaterial-embedded prototype. The metamaterial film embedded in polymer layers is separated from the ground metal plane and the top graphene sheet with different distances ($d_1 = 2\ \mu m, d_2 = 21\ \mu m$). The reflecting performance for three cases (GM absorber, single metamaterial, single graphene for $\mu_c = 0.2$ eV) is shown in Fig.5(a). It is noted that the lower resonant peak is mainly originated from the resonance of the metamaterial film. After integrating the metamaterial film into the graphene absorber, a strong absorbing peak turns up at this frequency. Moreover, the absorption performance can be artificially modulated by tuning the chemical potential. As shown in Fig. 5(b), the maximum absorption frequency shifts from 1.77 THz to 2.59 THz while varying chemical potentials from 0.2 eV to 0.8 eV. Besides, the reflection spectra exhibits extremely sharp valleys ($S11 < -36$ dB), indicating the promising applications of this GM absorber in sensors, modulators and filters, etc.

Compared with previous EM wave absorbers, the GM absorber in this work combines the advantages of graphene's tunable flexibility and metamaterial's sensitive frequency selectivity, opening up a distinct way to build graphene-metamaterial devices. Furthermore, modeling metamaterial elements as conductive sheets is an efficient methodology in considering multilayer dispersive media. Finally, to satisfy specific requirements in practice, one can employ other numerical optimization techniques (e.g., genetic algorithms) to deal with complex dispersion problems that will be faced in constructing multilayer GM device. This intuitional and concise circuit approach is also an ideal candidate to analyze the combined effects of metamaterial films and other current concerned two dimensional materials, such as monolayer 2D-SiC and silicene.

3. Conclusion

We have analytically investigated the circuit approach to integrate graphene and metamaterial in absorber design. Since the graphene sheet and the metamaterial film have relatively ultrathin optical thicknesses, their electrical properties are characterized via effective surface conductivity. Simulated results prove the validity of the transmission line model for GM absorber design. An optimized metamaterial-embedded structure is then proposed to build the frequency-tunable GM absorber depending on the chemical potential. Our work shows a feasible methodology to design tunable GM combined devices, which opens up new possibilities for further innovations in switchable optics.

Acknowledgements

This work was sponsored by the National Natural Science Foundation of China under Grants nos. 61322501, 61275183, 60990320 and 60990322, the National Program for Special Support of Top-Notch Young Professionals, the Foundation for the Author of National Excellent Doctoral Dissertation of the People's Republic of China under Grant no. 200950, the Program for New Century Excellent Talents (NCET-12–0489) in University, the K.P. Chao's High Technology Development Foundation, and the Fundamental Research Funds for the Central Universities (2014XZZX003-24).

References

[1] C.M. Watts, X.L. Liu, W.J. Padilla, Adv. Mater. 24 (2012) 98.
[2] B.A. Munk, Frequency Selective Surfaces: Theory and Design, John Wiley & Sons, New York, 2000.
[3] B.A. Munk, P. Munk, J. Pryor, IEEE Trans. Antennas Propag. 55 (2007) 186.
[4] S.A. Tretyakov, S.I. Maslovski, Microw. Opt. Technol. Lett. 38 (2003) 175.
[5] N.I. Landy, S. Sajuyigbe, J.J. Mock, D.R. Smith, W.J. Padilla, Phys. Rev. Lett. 100 (2008) 207402.
[6] X.J. He, Y. Wang, J.M. Wang, T.L. Gui, Q. Wu, Prog. Electromagn. Res. 115 (2011) 381.
[7] L. Huang, H. Chen, Prog. Electromagn. Res. 113 (2011) 103.
[8] M.H. Li, H.L. Yang, X.W. Hou, Y. Tian, D.Y. Hou, Prog. Electromagn. Res. 108 (2010) 37.
[9] B. Zhu, Z. Wang, C. Huang, Y. Feng, J. Zhao, T. Jiang, Prog. Electromagn. Res. 101 (2010) 231.
[10] S.A. Kuznetsov, A.G. Paulish, A.V. Gelfand, P.A. Lazorskiy, V.N. Fedorinin, Prog. Electromagn. Res. 122 (2012) 93.
[11] J.B. Pendry, A.J. Holden, W.J. Stewart, I. Youngs, Phys. Rev. Lett. 76 (1996) 4773.
[12] J.B. Pendry, A.J. Holden, D.J. Robbins, W.J. Stewart, IEEE Trans. Microw. Theory 47 (1999) 2075.
[13] H.S. Chen, L. Huang, X.X. Cheng, H. Wang, Prog. Electromagn. Res. 115 (2011) 317.
[14] S. Xu, L. Yang, L. Huang, H.S. Chen, Prog. Electromagn. Res. 120 (2011) 327.
[15] H.S. Chen, L.X. Ran, J.T. Huangfu, X.M. Zhang, K.S. Chen, T.M. Grzegorczyk, J.A. Kong, Prog. Electromagn. Res. 51 (2005) 231.
[16] H. Tao, N.I. Landy, C.M. Bingham, X. Zhang, R.D. Averitt, W.J. Padilla, Opt. Express 16 (2008) 7181.
[17] X.L. Liu, T. Starr, A.F. Starr, W.J. Padilla, Phys. Rev. Lett. 104 (2010) 207403.
[18] Y. Avitzour, Y.A. Urzhumov, G. Shvets, Phys. Rev. B 79 (2009) 045131.
[19] K. Aydin, V.E. Ferry, R.M. Briggs, H.A. Atwater, Nat. Commun. 2 (2011) 517.
[20] K.S. Novoselov, A.K. Geim, S.V. Morozov, D. Jiang, Y. Zhang, S.V. Dubonos, I.V. Grigorieva, A.A. Firsov, Science 306 (2004) 666.
[21] K.S. Novoselov, A.K. Geim, S.V. Morozov, D. Jiang, M.I. Katsnelson, I.V. Grigorieva, S.V. Dubonos, A.A. Firsov, Nature 438 (2005) 197.
[22] A.K. Geim, K.S. Novoselov, Nat. Mater. 6 (2007) 183.
[23] A. Vakil, N. Engheta, Science 332 (2011) 1291.
[24] L. Ju, B.S. Geng, J. Horng, C. Girit, M. Martin, Z. Hao, H.A. Bechtel, X.G. Liang, A. Zettl, Y.R. Shen, F. Wang, Nat. Nanotechnol. 6 (2011) 630.
[25] P.Y. Chen, A. Alu, ACS Nano 5 (2011) 5855.
[26] A.N. Grigorenko, M. Polini, K.S. Novoselov, Nat. Photonics 6 (2012) 749.
[27] R. Alaee, M. Farhat, C. Rockstuhl, F. Lederer, Opt. Express 20 (2012) 28017.
[28] A. Fallahi, J. Perruisseau-Carrier, Phys. Rev. B 86 (2012) 195408.
[29] H.G. Yan, X.S. Li, B. Chandra, G. Tulevski, Y.Q. Wu, M. Freitag, W.J. Zhu, P. Avouris, F.N. Xia, Nat. Nanotechnol. 7 (2012) 330.
[30] S. Thongrattanasiri, F.H.L. Koppens, F.J.G. de Abajo, Phys. Rev. Lett. 108 (2012) 047401.
[31] J.A. Kong, Electromagnetic Wave Theory, EMW publishing, Cambridge, MA, 2008.
[32] K.F. Mak, L. Ju, F. Wang, T.F. Heinz, Solid State Commun. 152 (2012) 1341.

[33] J.D. Buron, D.H. Petersen, P. Boggild, D.G. Cooke, M. Hilke, J. Sun, E. Whiteway, P.F. Nielsen, O. Hansen, A. Yurgens, P.U. Jepsen, Nano Lett. 12 (2012) 5074.
[34] L. Ren, Q. Zhang, J. Yao, Z.Z. Sun, R. Kaneko, Z. Yan, S. Nanot, Z. Jin, I. Kawayama, M. Tonouchi, J.M. Tour, J. Kono, Nano Lett. 12 (2012) 3711.
[35] T. Baba, Nat. Photonics 1 (2007) 11.
[36] G.W. Hanson, IEEE Trans. Antenna Propag. 56 (2008) 747.
[37] G.W. Hanson, J. Appl. Phys. 103 (2008) 064302.
[38] V.P. Gusynin, S.G. Sharapov, J.P. Carbotte, J. Phys.—Condens. Mat. 19 (2007) 026222.
[39] G.W. Hanson, J. Appli. Phys. 104 (2008) 084314.
[40] P. Tassin, T. Koschny, C. Soukoulis, Physica B 407 (2012) 4062.
[41] B. Sensale-Rodriguez, R.S. Yan, M.M. Kelly, T. Fang, K. Tahy, W.S. Hwang, D. Jena, L. Liu, H.G. Xing, Nat. Commun. 3 (2012) 780.
[42] A. Andryieuski, A.V. Lavrinenko, Opt. Express 21 (2013) 9144.